Simultaneous Fundus Imaging and Optical Coherence Tomography of the Mouse Retina

Omer P. Kocaoglu,[1,2] *Stephen R. Uhlhorn,*[1,2] *Eleut Hernandez,*[1] *Roger A. Juarez,*[1,2] *Russell Will,*[1,2] *Jean-Marie Parel,*[1,2] *and Fabrice Manns*[1,2]

Purpose. To develop a retinal imaging system suitable for routine examination or screening of mouse models and to demonstrate the feasibility of simultaneously acquiring fundus and optical coherence tomography (OCT) images.

Methods. The imaging system is composed of a photographic slit lamp for biomicroscopic examination of the fundus, an OCT interferometer, an OCT beam delivery system designed for the mouse eye, and a mouse positioning stage. Image acquisition was controlled with software that displays the fundus and OCT images in real time, and allows the user to control the position of the OCT beam spot on the fundus image display. The anesthetized mouse was placed in a cylindrical holder on the positioning stage, and a single operator adjusted the position of mouse.

Results. Fundus images and OCT scans were successfully acquired in both eyes of 8 C57BL/6 mice. Once the animal is anesthetized and placed in the holder, a typical imaging experiment takes less than 2 minutes. The retinal vasculature, pigmentation, nerve fiber arrangement, and optic nerve head were clearly visible on the fundus images. The quality of the OCT images was sufficient to allow measurement of the total, inner, and outer retinal thicknesses and to visualize the optic nerve head excavation.

Conclusions. The study demonstrates the feasibility of acquiring simultaneous fundus and OCT images of the mouse retina, by a single operator, in a manner suitable for routine evaluation of mouse models of retinal disease. (*Invest Ophthalmol Vis Sci.* 2007;48:1283–1289) DOI:10.1167/iovs.06-0732

The mouse has become the primary laboratory model for the study of ocular diseases. Mouse models are expected to play a vital role in research to understand the mechanism of and develop new genetic and pharmaceutical therapies for glaucoma,[1–9] retinal degeneration,[10–16] and retinal vascular diseases.[17–20] Quantitative assessment of retinal anatomy and morphology and of visual function is a critical fundamental step, to characterize disease phenotype, to monitor disease progression, or to evaluate the response to experimental therapies.[21,22] Electroretinography (ERG), fundus examination, and fluorescein angiography are used routinely in mice to correlate visual function with anatomic findings in vivo.[23] In addition, new techniques for noninvasive measurement of intraocular pressure (IOP) in mice will help investigate the role of IOP in mouse models of glaucoma.[24–26] Retinal morphology has been assessed noninvasively using techniques such as optical coherence tomography and scanning laser ophthalmoscopy, but acquiring images of the mouse in vivo with these techniques has been challenging and time consuming.[17,27,28] There is currently a need for an imaging system that allows the rapid acquisition of mouse retinal images in vivo in a routine fashion.

A quantitative imaging system suitable for routine in vivo assessment of the mouse retinal microstructure would make it possible to correlate structural changes with clinical fundus appearance, ERG findings and IOP in real time and at any desired time point in the same mouse. Being able to monitor total disease progression over time, in the same animal would significantly reduce experimental variability, increase the sensitivity of the corresponding tests, and avoid artifacts due to histologic preparation. The number of animals necessary to obtain statistical significance would be reduced considerably. A technique for rapid real-time evaluation of retinal morphology would also be suitable for high-volume experiments, such as genetic screening of mutant mice.[29] In addition, such a system would allow a direct comparison of retinal images acquired in a mouse model of a specific ocular disease or condition with images obtained clinically in human subjects. Such comparative tests would help provide a better understanding of the similarities and key differences between the human disease and the corresponding mouse model.[30,31]

Currently, the most suitable noninvasive imaging technique for this application is optical coherence tomography (OCT).[32] OCT can provide high-resolution, cross-sectional images of the retinal microstructure.[33] The basic feasibility of obtaining OCT images of the mouse retina has been demonstrated[34–36] (Shah SM et al. *IOVS* 2004;45:ARVO E-Abstract 2375; Ghanta RK et al. *IOVS* 2000;41:ARVO Abstract 900; Hartl I et al. *IOVS* 2001;42: ARVO Abstract 4252), but there are several challenges in developing a dedicated mouse retinal imaging system suitable for routine in vivo quantitative morphologic evaluation. It is difficult to align the mouse eye with the optical system due to the small size of the pupil, the large dioptric power of the mouse eye and the lack of voluntary fixation. Alignment must be rapid (within seconds) to minimize anesthesia time, avoid temporary cataract formation, and allow imaging of large numbers of animals within an acceptable time frame. It is therefore critical that the imaging system be optimized to minimize the positioning and alignment time.

One solution to the alignment problem for mouse OCT imaging is to obtain a real-time image of the mouse eye and the fundus for guidance. Providing a real-time image of the fundus also makes it possible to visualize the OCT spot on the fundus. Visualization of the OCT spot helps to control the OCT scan position. A true color fundus image also provides anatomic

From the [1]Ophthalmic Biophysics Center, Bascom Palmer Eye Institute, University of Miami Miller School of Medicine, Miami, Florida; and the [2]Biomedical Optics and Laser Laboratory, Department of Biomedical Engineering, University of Miami College of Engineering, Coral Gables, Florida.

Supported part by the Wollowick Foundation; NIH Grant R03 EY016322; NIH Grant F32 EY15636 (S. Uhlhorn); NIH Center Grant P30-EY014801; Research to Prevent Blindness, New York, NY; The Florida Lions Eye Bank, Miami, FL; The Henri and Flore Lesieur Foundation, West Palm Beach, FL.

Submitted for publication June 29, 2006; revised September 20 and October 16, 2006; accepted January 10, 2007.

Disclosure: **O.P. Kocaoglu**, None; **S.R. Uhlhorn**, None; **E. Hernandez**, None; **R.A. Juarez**, None; **R. Will**, None; **J.-M. Parel**, None; **F. Manns**, None

The publication costs of this article were defrayed in part by page charge payment. This article must therefore be marked "*advertisement*" in accordance with 18 U.S.C. §1734 solely to indicate this fact.

Corresponding author: Fabrice Manns, Bascom Palmer Eye Institute; 1638 NW 10th Avenue, Miami, FL 33136; fmanns@miami.edu.

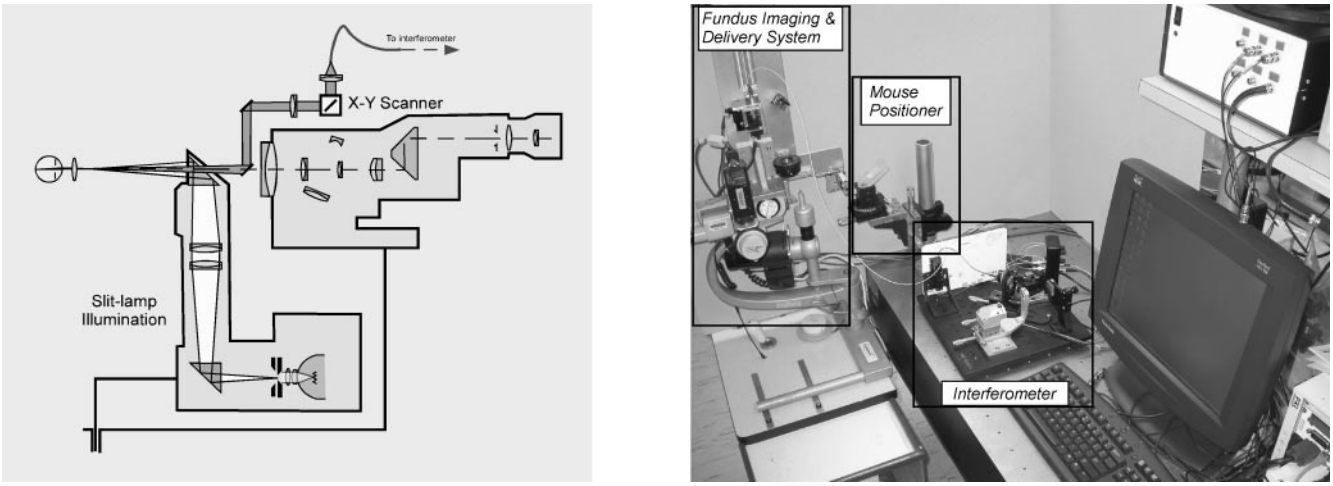

FIGURE 1. *Left*: general optical design of the imaging system; *right*: the mouse fundus and OCT imaging system, including fundus imaging with a digital camera attached to the photographic port of the slit lamp, the OCT beam delivery system, the six-axis mouse positioner, and the interferometer.

information on pigmentation and vasculature of the retina that is useful for phenotyping or disease characterization.

Several techniques have been used to acquire fundus images of the mouse eye. Hawes et al.[31] developed a procedure to obtain high-quality mouse fundus images with a small animal fundus camera (Genesis, Kowa, Japan) and an auxiliary lens. A human fundus camera or a slit lamp and an auxiliary lens can also be used.[2,37] Another common approach is the applanation of the mouse cornea with a microscope cover glass to cancel its optical effect. The fundus can then be visualized with a dissecting microscope or slit lamp biomicroscope, either directly or through a low-power auxiliary lens.[21] Cohan et al.[38] developed a custom-made Goldmann-type contact lens to image the mouse optic disc with a slit lamp biomicroscope equipped with a digital camera. The contact lens cancels most of the dioptric effect of the anterior corneal surface without requiring applanation. The mouse fundus imaging technique that is most compatible for integration into an OCT and fundus imaging system is the use of a slit lamp biomicroscope with an auxiliary lens. On the one hand, the slit lamp provides a platform that is more flexible and more easily adaptable than a commercial fundus camera. On the other hand, canceling the corneal power by applanation or with a contact lens makes it more difficult to acquire a fundus and OCT images simultaneously.

The goal of the present study was to demonstrate the feasibility of simultaneously acquiring fundus and OCT images in the mouse. In this report, the development of a noncontact slit lamp–based instrument and method is presented. A special emphasis is placed on designing a system suitable for rapid examination or screening of mouse models.

MATERIALS AND METHODS

General Description

The system includes four main components: a photographic slit lamp (focal length [f] = 125 mm; Carl Zeiss Meditec, GmbH, Oberkochen, Germany) for biomicroscopic examination of the fundus with an auxiliary lens, an OCT interferometer, an OCT beam delivery system designed for the mouse eye and mounted on the slit lamp, and a mouse positioning stage (Fig. 1). The OCT and fundus imaging systems are coupled with an aluminum mirror that is mounted at 45° in front of the slit lamp microscope objective, so as to be located between the two observation channels of the slit lamp (Fig. 1). The image acquisition is controlled with custom-made software that displays the fundus image and the OCT image in real time, and allows the user to control the position of the OCT beam spot on the fundus image display.

Interferometer

The OCT system is a time-domain system with a superluminescent diode (SLD 371; Superlum, Moscow, Russia) with a center wavelength of 830 nm, a bandwidth of 45 nm, and an output power of 6 mW. The power delivered to the mouse eye was 700 μW. The reference arm of the interferometer is a grating-based dispersive optical delay line that performs 2-mm depth scans at a speed of 400 A-lines/s with up to 2000 points per line. Typical images consist of 400 to 800 lines. The interference signal is band-pass filtered and recorded by a 12-bit data acquisition board and the full-fringe data were used to process, demodulate, and display the final OCT image. The axial resolution of the OCT system measured in air, when using a mirror as the sample arm, is 8 μm. The sensitivity measured by recording the signal produced when a mirror and adjustable neutral density filter is placed in the sample arm is 88 dB.

Fundus Imaging

Fundus images were acquired by mounting an auxiliary lens in front of the slit lamp at a fixed distance from the objective. The auxiliary lens creates an aerial image of the fundus in the focal plane of the slit lamp objective. The slit lamp objective and auxiliary lens form a telescopic system. A reduced paraxial optical model of the mouse eye was developed to select the power of the auxiliary lens (Juarez RA et al. *IOVS* 2004;45:ARVO E-Abstract 2788). Based on these calculations, a 90-D lens (AE111371; Volk, Mentor, OH) was selected to provided a 2-mm retinal field of view (Fig. 2). The mouse retina was illuminated using the white-light illumination system of the slit lamp. The slit was opened to provide wide-field illumination. The light beam was delivered through the lens. Fundus images are recorded with a color digital camera (XCD-SX910CR; Sony, Park Ridge, NJ) attached to the photographic port of the slit lamp. The camera also allowed real-time visualization of the mouse eye during alignment and centering.

Delivery System

A telecentric scanning delivery system was designed to scan the OCT beam onto the mouse retina. The delivery system consists of a fiber-optic collimator (PAF-X-7-λ; OFR, Caldwell, NJ) that produces a 1.6-mm diameter beam, a set of galvanometer scanners (6220H; Cambridge Technologies, Cambridge, MA), and a scanning lens (F = 200 mm) that focuses the OCT beam in the focal plane of the 90-D lens (Fig. 3). To allow precise alignment and provide adequate mechanical stability, the

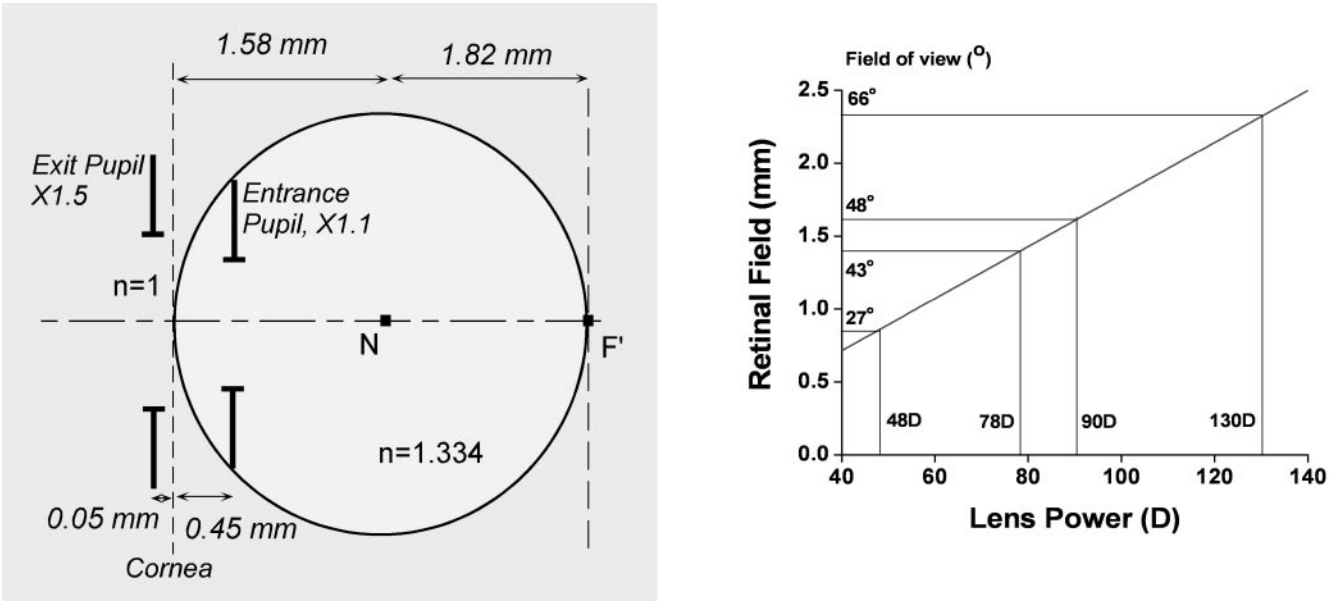

FIGURE 2. *Left*: reduced paraxial model of the mouse eye. The model was used to calculate the field of view as a function of auxiliary lens power, and it was derived from the complete paraxial model of Remtulla and Hartlett.[39] *Right*: The model predicts that 90-D auxiliary lens provides a field of view of approximately 48°.

OCT beam delivery system was mounted on a custom-made aluminum plate that was firmly mounted on the slit lamp with an angle bracket.

Mouse Positioner

A six-axis mouse positioner consisting of two goniometer stages (123-2745; Optosigma Corp., Santa Ana, CA), a rotation stage (124-0050/0055, Optosigma Corp.), and three linear translation stages (UMR8.25; NewPort, Irvine, CA) was designed to position the mouse precisely and align the optical axis of the mouse eye with the axis of the delivery system. The mouse was held in a cylindrical holder made from 30-mL syringes. The holder was mounted on the stage and designed to facilitate delivery of the beam to the mouse eye (Fig. 4).

Imaging Procedure

In a first set of experiments designed to test the functionality of the system, three healthy C57BL/6 mice (Jackson Laboratory, Bar Harbor, ME) were imaged at various time intervals between 3 and 7 months of age. In a second set of experiments designed to quantify the intersession variability, five healthy C57BL/6 (Jackson Laboratory) mice were imaged at 3 and 4 weeks of age. These mice were euthanized at 4 weeks after the second imaging session, and the eyes were prepared for histologic analysis. All animals were treated in accordance with the ARVO Statement for Use of Animals in Ophthalmic and Vision Research. The Committee and Review Board for Animal Research of the

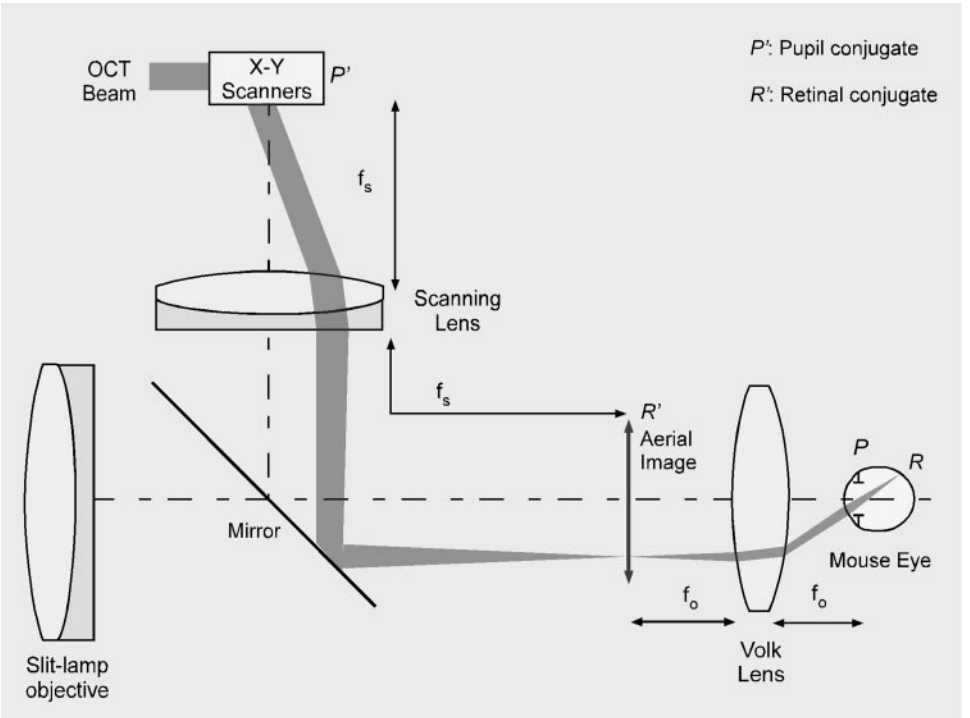

FIGURE 3. The OCT beam delivery system, where R is the retinal plane, P is the pupil plane, P′ is the conjugate of the pupil plane, R′ is the conjugate of the retinal plane, f_s is the focal length of the scanning lens, and f_o is the focal length of the objective lens. The delivery system is calculated to produce a retinal spot size on the order of 10 μm (f_s = 200 mm, f_o = 11 mm).

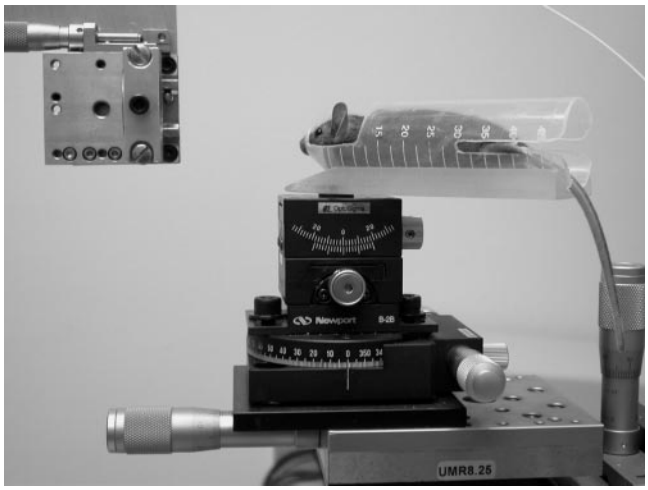

FIGURE 4. The mouse was held in a cylindrical holder made from 30-mL syringes. The position of the mouse was adjusted to align the optical axis of the mouse eye with the axis of the delivery system by using 6-μm screws.

University of Miami, Miller School of Medicine approved all animal studies. The iris was dilated by topical administration of 1% tropicamide. After the pupil was dilated, the animals were anesthetized with a 0.5 to 0.7-mL/kg intramuscular injection of 42.8 mg/mL ketamine, 8.5 mg/mL xylazine, and 1.4 mg/mL acepromazine. To avoid dehydration and loss of ocular transparency,[31,38] the mouse cornea was irrigated at regular intervals (approximately every 2 minutes) with a 0.2-mm-bore soft cannula filled with physiologic saline (Balanced Salt Solution [BSS]; Alcon, Fort Worth, TX).

The anesthetized mouse was placed in the cylindrical holder and mounted in front of the imaging system on the positioning stage. A single operator adjusted the position of the animal using the real-time video display of the eye and fundus for guidance. The alignment consisted of two steps. The position of the mouse was first coarsely adjusted until a view of the retina was obtained. The mouse was then moved toward the objective, and precisely aligned until a clear image of the fundus filled the screen and the OCT spot was visualized. The position of the OCT spot on the retina was then adjusted using the control software, and an image of the area of interest was acquired.

At the end of the imaging session, the animal was returned to its cage or euthanatized for histology. After the last imaging experiment, while under deep anesthesia, the mouse was placed in a chamber and euthanatized by CO_2 fume inhalation. This method is consistent with the recommendation of the panel on Euthanasia of the American Veterinary Medical Association. The globe was enucleated, immersed in fixative, embedded in paraffin, and sectioned for histologic analysis. Light microscopy of histologic sections stained with hematoxylin and eosin was used to identify the anatomic structures and boundaries detected in the OCT images.

Retinal Thickness Measurements

The control software of the imaging system saves the digital fundus image and the raw OCT image signal in exportable data files. A program written in commercial software (MatLab, ver. 7.0; The MathWorks, Natick, MA) is used to process the raw image data and display the final image. Thickness measurements are performed manually on randomly selected A-lines in the region of interest. The position of the intensity peaks corresponding to the boundaries of interest is determined from the numerical values of the A-line signals. Inner retinal thickness is measured from the intensity peak corresponding to the interface of the vitreous and nerve fiber layer (NFL), to the intensity peak corresponding to the interface between the inner nuclear (INL) and outer plexiform (OPL) layers. Outer retinal thickness is measured from the intensity peak corresponding to the interface between the INL and OPL, to the intensity peak, which corresponds to the interface between the photoreceptor layer (PL) and retinal pigment epithelium (RPE; Fig. 5). In each image, the thickness was measured along two to five A-lines at two to three optic disc diameters away from the optic disc.

The intrasession variability was determined by calculating the average and standard deviation of the thickness obtained in five to nine successive images. The intersession variability was quantified by calculating the thickness difference in images acquired from the same eye in two different sessions.

RESULTS

Fundus images and OCT scans were successfully acquired in both eyes of all eight C57BL/6 mice (Fig. 6). On average, once the animal was anesthetized and placed in the holder, a typical imaging experiment was completed in less than 2 minutes. The duration of the OCT scan was 1 second (400 lines per image, acquired at 400 lines/s).

The retinal vasculature, pigmentation, and nerve fiber arrangement and optic nerve head could be clearly visualized on the fundus images (Figs. 6, 7). The quality of the OCT images is sufficient to allow measurement of the total, inner, and outer retinal thicknesses and to visualize the optic nerve head excavation (Figs. 5, 6, 7, Table 1). Additional retinal layers were detectable, but the dynamic range of the image (approximately 27 dB) was not sufficient to obtain a clear image of the detailed anatomic structure of the mouse retina. The large scan depth allowed imaging of the entire posterior segment, including the

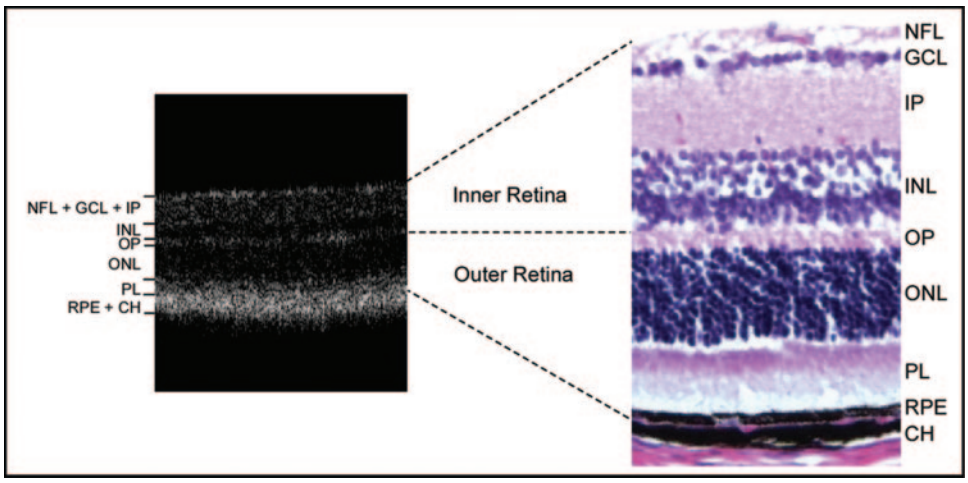

FIGURE 5. Comparison of OCT image and histologic image of a 4-week-old female C57BL/6 mouse. The retinal layers can be distinguished, but not with sufficient sensitivity to allow reliable quantitative analysis of individual layers. GCL, ganglion cell layer; IPL, inner plexiform layer; INL, inner nuclear layer; OPL, outer plexiform layer; ONL, outer nuclear layer; PL; RPE, retinal pigment epithelium; CH, choroid.

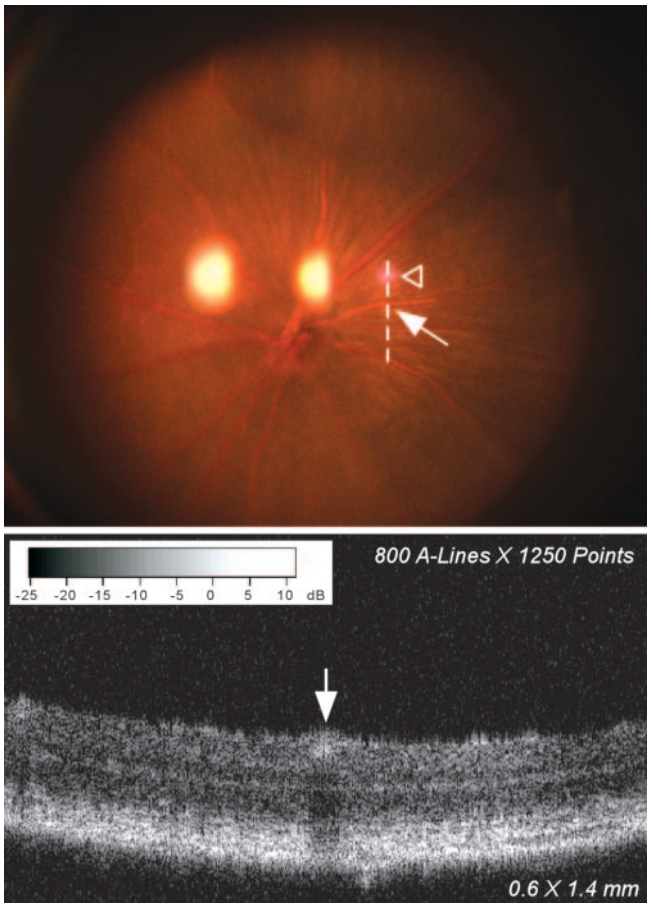

FIGURE 6. *Top*: Fundus image of a 3-month-old female C57BL/6 mouse recorded simultaneously with the OCT image. The OCT scan was acquired on a vertical line shown on the fundus image (*dashed line*). The OCT beam spot (*triangle*) and the blood vessel (*arrow*) appear on the fundus image. *Bottom:* OCT scan of the same C57BL/6 mouse. Total retinal thickness and inner and outer retinal separation can be seen on the OCT scan. *Arrow*: blood vessel.

posterior part of the lens, the vitreous, and retina (Fig. 8). The use of the 90-D lens helped produce large lateral scans, covering up to approximately 2 mm on the mouse retina, which corresponds to a field of view of approximately 48°.

The axial resolution of the images, quantified by measuring the full-width at half maximum (FWHM) of the interference peaks along selected A-lines, was found to be approximately 12 μm. The intravisit variability of the retinal thickness measurements was less than 5% (Table 1) and the intervisit variability at a 1-week interval was less than 6% (Table 1).

DISCUSSION

Our experiments demonstrate the feasibility of acquiring simultaneous fundus and OCT images of the mouse eye in a time suitable for routine evaluation of mouse models of retinal diseases. The emphasis of the design was to develop a technique and device that allow a single trained operator to rapidly (within minutes) acquire mouse retinal images. Three key design features helped to solve this issue. First, the mouse holder and positioning stage allowed precise alignment and positioning of the mouse eye by a single operator. Second, the position of the slit lamp and auxiliary lens were fixed, so that only the mouse position needed to be adjusted. Finally, the real-time video image of the eye and fundus helped to guide the alignment.

The slit lamp–based delivery system produced high-quality, wide-field fundus images and wide-field OCT images of sufficient quality to allow measurements of inner, outer, and total retinal thickness and of the optic nerve head excavation with a resolution on the order of 10 μm. The intravisit and intervisit variability of the retinal thickness measurements was on the order of 10 μm. Since the retinal thickness of C57Bl/6 mice is not expected to change significantly in 1 week, these results indicate that the current system can detect changes in thickness on the order of 10 μm between different time points in a longitudinal study. The dynamic range of the images was not sufficient to allow a computerized segmentation of the retinal layers. A manual technique was therefore used to measure the retinal thickness on A-lines that were randomly selected within the region of interest. The exact position of the intensity peaks was detected by inspection of the A-line signals. The manual technique minimizes the error in the detection of the intensity peaks. It therefore represents the highest reproducibility that can be achieved with the imaging system.

Our retinal thickness measurements (178 $\pm$ 4 μm) are consistent with those obtained by Horio et al.[35] using OCT (174 $\pm$ 5 μm) and by Schmucker and Schaeffel[40] on frozen sections (170–180 μm) in mice of the same age. Using OCT, Li et al.[34] found significantly thicker retinas for healthy mice (220–250 μm). Their OCT measurements are also more than

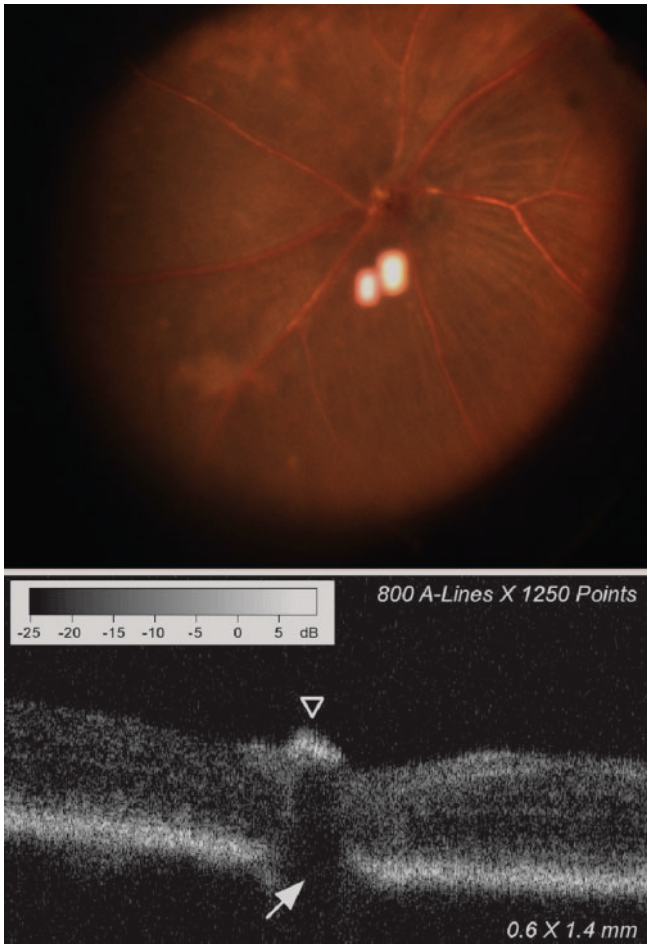

FIGURE 7. *Top:* Fundus image of a 3-month-old female C57BL/6 mouse recorded simultaneously with the OCT during the same experiment. *Bottom*: OCT scan of the same C57BL/6 mouse through the optic nerve head. Total retinal thickness and inner and outer retinal separation, optic nerve head (*arrow*) can be seen on the OCT scan. *Triangle*: central retinal artery.

TABLE 1. Retinal Thickness in Five C57BL/6 Mice Imaged at 3 and 4 Weeks of Age

		Age: Week 3 (μm)	Age: Week 4 (μm)	Difference (μm)	Difference (%)
1	Inner retina	89 ± 3	90 ± 4	1	1.1
	Outer retina	92 ± 4	91 ± 4	−1	−1.0
	Total retina	182 ± 5	181 ± 6	−1	−0.5
2	Inner retina	85 ± 2	89 ± 3	4	4.5
	Outer retina	87 ± 3	92 ± 5	5	5.4
	Total retina	172 ± 3	180 ± 6	8	4.4
3	Inner retina	87 ± 3	82 ± 2	−5	−6.0
	Outer retina	90 ± 4	91 ± 3	1	1.0
	Total retina	177 ± 5	173 ± 3	−4	−2.3
4	Inner retina	86 ± 3	84 ± 3	−2	−2.3
	Outer retina	92 ± 2	92 ± 5	0	0.0
	Total retina	178 ± 3	176 ± 5	−2	−1.1
5	Inner retina	89 ± 3	88 ± 4	−1	−1.1
	Outer retina	92 ± 3	94 ± 7	2	2.1
	Total retina	182 ± 2	181 ± 9	−1	−0.5
Average	Inner retina	87 ± 2	87 ± 3	0	0.0
	Outer retina	90 ± 2	92 ± 1	2	2.1
	Total retina	178 ± 4	178 ± 4	0	0.0

Each value corresponds to the average of measurements performed on five to nine successive images at a distance of two to three optic disc diameters from the optic disc.

twice the values that they obtained with histology. The reason for this discrepancy is unclear.

The current OCT system uses a standard time-domain implementation.[34,35] In principle, higher resolution and higher sensitivity images providing additional structural detail can be obtained using recently developed ultra–high-resolution and high-speed OCT technology (spectral-domain OCT). When used with broadband sources that provide improved resolution, spectral-domain OCT can produce retinal images in human eyes with a resolution on the order of 4 μm and a sensitivity of 95 dB, at a rate of nearly 30,000 lines/s.[41,42] The high speed provided by the spectral-domain approach allows the acquisition of three-dimensional images. There have been several unpublished reports of the use of this technology for mouse imaging (Shah SM, et al. *IOVS* 2004;45:ARVO E-Abstract 2375; Kim K et al. *IOVS* 2006;47:ARVO E-Abstract 2923). Even though the OCT interferometer of the present study used a conventional time-domain approach, the delivery system is compatible with spectral domain OCT. In principle, because of the modular design of the slit lamp based system, the only change that is required to upgrade the system to spectral-domain is to modify the design of the OCT interferometer and control software. A high-speed spectral domain approach may be desirable, particularly since mouse retinal OCT is more prone to motion artifacts during conventional OCT imaging due to small size and the high dioptric power of the mouse eye and the higher breathing and heart rates.

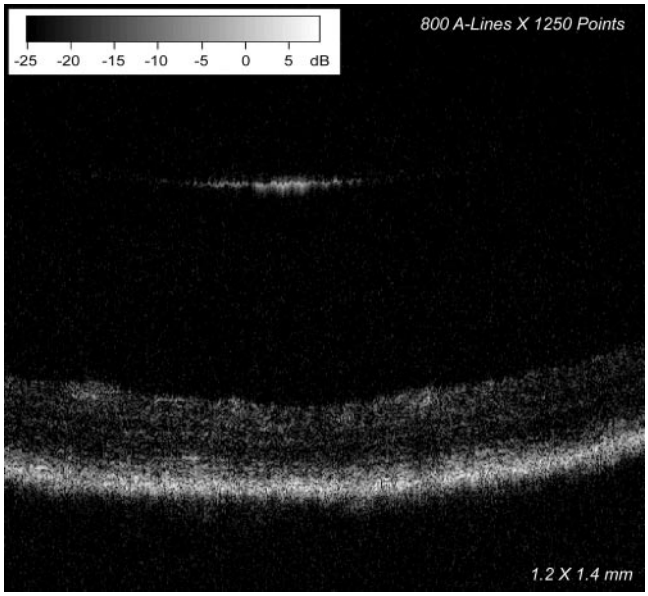

FIGURE 8. OCT scan of a 7-month-old female C57BL/6 mouse showing the posterior crystalline lens and retina.

In the end, however, the resolution and quality of mouse OCT images may be inherently limited by problems related to the optical quality and refractive state of the mouse eye. There is evidence that the optical quality of the mouse eye is significantly lower than that of the human eye, with a large variability between animals.[43,44] In addition, Remtulla and Hallett[39] found that the mouse eye has a large amount of chromatic aberration. There is also evidence that the mouse eye is slightly hyperopic and that its paraxial optical characteristics change significantly with age due to lens growth and changes in its axial length.[40,45] Burns et al. (*IOVS* 2004;45:ARVO E-Abstract 2787) and Lin et al. (*IOVS* 2004;45:ARVO E-Abstract 2786) also found that the refractive error varies significantly between animals and that a large range of defocus compensation was necessary to acquire scanning laser ophthalmoscope (SLO) images in mice. Defocus, monochromatic aberrations, and chromatic aberrations may limit the resolution and signal-to-noise ratio that can be achieved with OCT in the mouse eye, particularly when imaging older or diseased animals. Even if the resolution and sensitivity are not sufficient to resolve the retinal microstructure in the mouse eye with low optical quality, OCT can still provide useful quantitative data in studies requiring noninvasive thickness measurements.

The goal of the present study was to demonstrate the technical feasibility of acquiring simultaneous fundus and OCT images of the mouse in vivo. Experiments were conducted in healthy mice to demonstrate this feasibility. The importance and applicability in routine animal research cannot be fully demonstrated until complete studies are performed in diseased animal models. However, the experiments and data presented herein demonstrate the potential of such a system.

Acknowledgments

The authors thank Vittorio Porciatti, PhD, Robert Knighton, PhD, George Inana, MD, PhD, Shuliang Jiao, PhD, Abigail Hackam, PhD, and Carmen Puliafito, MD, MBA, for scientific input and technical assistance and David Denham, MSME, for technical assistance.

References

1. Grozdanic SD, Kwon YH, Sakaguchi DS, Kardon RH, Sonea IM. Functional evaluation of retina and optic nerve in the rat model of chronic ocular hypertension. *Exp Eye Res*. 2004;79:75–83.
2. Bayer AU, Brodie SE, Mittag T. Pilot study of pattern-electroretinographic changes in the DBA/2NNia mouse: animal model of congenital angle-closure glaucoma. *Ophthalmologe*. 2001;98:248–252.
3. Libby RT, Smith RS, Savinova OV, et al. Modification of ocular defects in mouse developmental glaucoma models by tyrosinase. *Science*. 2003;299:1578–1581.
4. Mabuchi F, Aihara M, Mackey MR, Lindsey JD, Weinreb RN. Regional optic nerve damage in experimental mouse glaucoma. *Invest Ophthalmol Vis Sci*. 2004;45:4352–4358.
5. Schuettauf F, Quinto K, Naskar R, Zurakowski D. Effects of antiglaucoma medications on ganglion cell survival: the DBA/2J mouse model. *Vision Res*. 2002;42:2333–2337.
6. May CA, Mittag T. Neuronal nitric oxide synthase (nNOS) positive retinal amacrine cells are altered in the DBA/2NNia mouse, a murine model for angle-closure glaucoma. *J Glaucoma*. 2004;13:496–499.
7. Inman DM, Sappington RM, Horner PJ, Calkins DJ. Quantitative correlation of optic nerve pathology with ocular pressure and corneal thickness in the DBA/2 mouse model of glaucoma. *Invest Ophthalmol Vis Sci*. 2006;47:986–996.
8. Matsubara A, Nakazawa T, Husain D, et al. Investigating the effect of ciliary body photodynamic therapy in a glaucoma mouse model. *Invest Ophthalmol Vis Sci*. 2006;47:2498–2507.
9. Dyka FM, May CA, Enz R. Subunits of the epithelial sodium channel family are differentially expressed in the retina of mice with ocular hypertension. *J Neurochem*. 2005;94:120–128.
10. Ambati J, Anand A, Fernandez S, et al. An animal model of age-related macular degeneration in senescent Ccl-2 or Ccr-2 deficient mice. *Nat Med*. 2003;9:1390–1397.
11. Rakoczy EP, Yu MJ, Nusinowitz S, Chang B, Heckenlively JR. Mouse models of age-related macular degeneration. *Exp Eye Res*. 2006;82:741–752.
12. Chang B, Hawes NL, Hurd RE, Davisson MT, Nusinowitz S, Heckenlively JR. Retinal degeneration mutants in the mouse. *Vision Res*. 2002;42:517–525.
13. Samardzija M, Wenzel A, Naash M, Reme CE, Grimm C. Rpe65 as a modifier gene for inherited retinal degeneration. *Eur J Neurosci*. 2006;23:1028–1034.
14. Linberg KA, Fariss RN, Heckenlively JR, Farber DB, Fisher SK. Morphological characterization of the retinal degeneration in three strains of mice carrying the rd-3 mutation. *Vis Neurosci*. 2005;22:721–734.
15. Shearstone JR, Wang YE, Clement A, et al. Application of functional genomic technologies in a mouse model of retinal degeneration. *Genomics*. 2005;85:309–321.
16. Roderick TH, Chang B, Hawes NL, Heckenlively JR. A new dominant retinal degeneration (Rd4) associated with a chromosomal inversion in the mouse. *Genomics*. 1997;42:393–396.
17. Xu H, Manivannan A, Goatman KA, et al. Improved leukocyte tracking in mouse retinal and choroidal circulation. *Exp Eye Res*. 2002;74:403–410.
18. Heckenlively JR, Hawes NL, Friedlander M, et al. Mouse model of subretinal neovascularization with choroidal anastomosis. *Retina*. 2003;23:518–522.
19. Clements RS Jr, Robison WG Jr, Cohen MP. Anti-glycated albumin therapy ameliorates early retinal microvascular pathology in db/db mice. *J Diabetes Complications*. 1998;12:28–33.
20. Shen D, Wen R, Tuo J, Bojanowski CM, Chan CC. Exacerbation of retinal degeneration and choroidal neovascularization induced by subretinal injection of Matrigel in CCL2/MCP-1-deficient mice. *Ophthalmic Res*. 2006;38:71–73.
21. Pinto LH, Enroth-Cugell C. Tests of the visual mouse system. *Mamm Genome*. 2000;11:531–536.
22. Smith RS, Korb D, John SWM. A goniolens for clinical monitoring of the mouse iridocorneal angle and optic nerve. *Mol Vis*. 2002;8:26–31.
23. Smith RS, ed. *Systematic Evaluation of the Mouse Eye: Anatomy, Pathology and Biomethods.* Boca Raton, FL: CRC Press; 2002.
24. Reitsamer HA, Kiel JW, Harrison JM, Ransom NL, McKinnon SJ. Tonopen measurement of intraocular pressure in mice. *Exp Eye Res*. 2004;78:799–804.
25. Danias J, Kontiola AI, Filippopoulos T, Mittag T. Method for the noninvasive measurement of intraocular pressure in mice. *Invest Ophthalmol Vis Sci*. 2003;44:1138–1141.
26. Cohan BE, Bohr DF. Measurement of intraocular pressure in awake mice. *Invest Ophthalmol Vis Sci*. 2001;42:160–163.
27. Paques M, Simonutti M, Roux MJ, et al. High resolution fundus imaging by confocal scanning laser ophthalmoscopy in the mouse. *Vision Res*. 2006;46:1336–1345.
28. Ruether K, van de Pol D, Jaissle G, Berger W, Tornow RP, Zrenner E. Retinoschisislike alterations in the mouse eye caused by gene targeting of the Norrie disease gene. *Invest Ophthalmol Vis Sci*. 1997;38:710–718.
29. Pinto LH, Hotz Vitaterna M, et al. Results from screening over 9000 mutation-bearing mice in the electroretinogram and appearance of the fundus. *Vision Res*. 2004;44:3335–3345.
30. Kobayashi A, Higashide T, Hamasaki D, et al. HRG4 (UNC119) mutation found in cone-rod dystrophy causes retinal degeneration in a transgenic model. *Invest Ophthalmol Vis Sci*. 2000;41:3268–3277.
31. Hawes NL, Smith RS, Chang B, Davisson M, Heckenlively JR, John SWM. Mouse fundus photography and angiography: a catalogue of normal and mutant phenotypes. *Mol Vis*. 1999;5:22.
32. Huang D, Swanson EA, Lin CP, et al. Optical coherence tomography. *Science*. 1991;254:1178–1181.
33. Drexler W, Morgner U, Ghanta RK, Kartner FX, Schuman JS, Fujimoto JG. Ultrahigh-resolution ophthalmic coherence tomography. *Nat Med*. 2001;7:502–507.
34. Li Q, Timmers AM, Hunter K, et al. Noninvasive imaging by optical coherence tomography to monitor retinal degeneration in the mouse. *Invest Ophthalmol Vis Sci*. 2001;42:2981–2989.
35. Horio N, Kachi S, Hori K, et al. Progressive change of optical coherence tomography scans in retinal degeneration slow mice. *Arch Ophthalmol*. 2001;119:1329–1332.
36. Ko TH, Adler DC, Fujimoto JG, et al. Ultrahigh resolution optical coherence tomography imaging with a broadband superluminescent diode light source. *Opt Express*. 2004;12:2112–2119.
37. DiLoreto D, Grover DA, del Cerro C, del Cerro M. A new procedure for the fundus photography and fluorescein angiography in small laboratory animal eyes. *Curr Eye Res*. 1994;13:157–161.
38. Cohan BE, Pearch AC, Jokelainen PT, Bohr DF. Optic disc imaging in conscious rats and mice. *Invest Ophthalmol Vis Sci*. 2003;44:2560–2562.
39. Remtulla S, Hallett PE. A schematic eye for the mouse, and comparisons with the rat. *Vision Res*. 1985;25:21–31.
40. Schmucker C, Schaeffel F. A paraxial schematic eye model for the growing C57BL/6 mouse. *Vision Res*. 2004;44:1857–1867.
41. Jiao S, Knighton R, Huang X, Gregori G, Puliafito CA. Simultaneous acquisition of sectional and fundus ophthalmic images with spectral-domain optical coherence tomography. *Opt Express*. 2005;13:444–452.
42. Leitgeb R, Drexler W, Unterhuber A, et al. Ultrahigh resolution Fourier domain optical coherence tomography. *Opt Express*. 2004;12:2156–2165.
43. de la Cera EG, Rodriguez G, Llorente L, Schaefel F, Marcos S. Optical aberrations in the mouse eye. *Vision Res*. 2006;46:2546–2553.
44. Artal P, Herreros de Tejada P, Munoz Tedo C, Green D. Retinal image quality in the rodent eye. *Vis Neurosci*. 1998;15:597–605.
45. Schmucker C, Schaeffel F. In vivo biometry in the mouse eye with low coherence interferometry. *Vision Res*. 2004;44:2445–2456.